Modelling Global Trade
with Optimal Transport

Thomas Gaskin[1,2]*, **Marie-Therese Wolfram[3]**, **Andrew Duncan[2,4]**, **Guven Demirel[5]**

[1] Department of Applied Mathematics and Theoretical Physics, University of Cambridge, Cambridge CB3 0WA, United Kingdom; [2] Department of Mathematics, Imperial College London, London SW7 2AZ, United Kingdom; [3] Mathematics Institute, University of Warwick, Coventry CV4 7AL, UK; [4] The Alan Turing Institute, London NW1 2DB, United Kingdom; [5] School of Business and Management, Queen Mary University of London, London E1 4NS, United Kingdom

Correspondence: *trg34@cam.ac.uk

Abstract Global trade is shaped by a complex mix of factors beyond supply and demand, including tangible variables like transport costs and tariffs, as well as less quantifiable influences such as political and economic relations. Traditionally, economists model trade using gravity models, which rely on explicit covariates but often struggle to capture these subtler drivers of trade. In this work, we employ optimal transport and a deep neural network to learn a time-dependent cost function from data, without imposing a specific functional form. This approach consistently outperforms traditional gravity models in accuracy while providing natural uncertainty quantification. Applying our framework to global food and agricultural trade, we show that the global South suffered disproportionately from the war in Ukraine's impact on wheat markets. We also analyze the effects of free-trade agreements and trade disputes with China, as well as Brexit's impact on British trade with Europe, uncovering hidden patterns that trade volumes alone cannot reveal.

Keywords Food and Agricultural Trade, Optimal Transport, Econometrics, Neural Networks, Deep Learning

Contents

Introduction

International trade serves as the backbone of the world economy, distributing goods and connecting markets through global logistics networks. Its dynamics are driven by numerous factors beyond mere supply and demand, such as tariffs, non-tariff policy barriers, political and economic tensions, and disruptions caused by accidents, conflicts, and civil wars. Among all traded commodities, agricultural and food products hold particular interest for policymakers and the general public due to their significant volume, high trade value, and critical role in food security and resilience [1, 2]. Consumer food prices are a product of all the complexly interwoven factors governing trade. However, they do not always directly reflect the ease of doing business between any two countries. For instance, in May 2020, China imposed an 80% tariff on Australian barley, leading to a major restructuring of global supply chains (see fig. 4): Chinese demand was suddenly met from France, Canada, and Argentina, while Australia started exporting surplus barley e.g. to Saudi Arabia. Despite these shifts, for the next five months the global barley price barely budged [3, 4].

Modelling global trade has garnered significant attention in the economic literature, with *gravity models* being the most widely used approach [5–9]. These models, named for their direct analogy to Newton's law of gravity, assume that the total trade T_{ij} of a given commodity between two countries i and j is proportional to the total output O_i of the source country and the total expenditure E_j of the destination country, as well as inversely related to a 'distance' between them:

$$T_{ij}(t) \sim \frac{O_i(t)E_j(t)}{C_{ij}(t)}. \qquad (1)$$

This distance C_{ij} comprises all factors that contribute to the ease of selling goods produced in one country to another, including transportation costs, information costs, and tariff and non-tariff barriers to trade. Traditional gravity models use a set of covariates to estimate C_{ij} as

$$\log C_{ij}(t) = \sum_k \alpha_k \pi_{i,k}(t) + \sum_l \beta_l \chi_{j,l}(t)$$
$$+ \sum_m \gamma_m \rho_{ij,m}(t), \qquad (2)$$

where π_i and χ_j are exogenous exporter and importer-side regressors [10], ρ_{ij} are bilateral covariates, and α, β, γ are the coefficient vectors. Commonly used covariates include geographic proximity, the existence of trade agreements, colonial ties, tariffs, non-tariff barriers, or shared languages [11]. The *structural gravity model* corrects eq. (1) with import and export multilateral resistance terms, which account for the relative nature of bilateral trade shares. This adjustment has been shown to align with various microeconomic models [7]. Gravity models have been widely used to study agrifood trade. For instance, [12] estimate residual trade costs based on a micro-founded gravity equation, finding ad valorem costs to be 60% higher in the global South compared to the North. Studies have also investigated the impact of global and regional trade agreements [13,14] and the effect of eliminating tariffs [15, 16].

The gravity-based approach is attractive to researchers due to its interpretability, mathematical simplicity, and consistency with various microeconomic theories [9]. However, it is not without its limitations. For one, multilateral trade resistance terms, central to the structural gravity model, are unobservable and must be estimated, often using fixed effects. Elasticity and other key parameters are often unavailable at a granular level, requiring aggregation that can introduce bias [17]. The model's cost function also depends heavily on the choice of covariates and functional form, making specification crucial for interpreting results. In addition, unobservables—such as the subtle effects of changing political relations, public preferences, or aversions toward products from specific countries—are absorbed in the error term. Finally, while trade costs are generally asymmetric ($C_{ij} \neq C_{ji}$), commonly used covariates are not, making it difficult for a model to capture the inherent imbalances in trade relationships. See [9, 11, 18] for a deeper discussion of challenges and best practices.

In this work, we present a more general approach that dispenses with the use of covariates and a functional form, instead inferring the cost directly from data. Our method is based on the *optimal transport* (OT) framework [19], which generalises gravity-based models. In OT, trade flows are assumed to match supply and demand to minimise an overall cost. Mathematically, this is expressed as follows: let $\mathbf{C} \in \mathbb{R}^{m \times n}$ be a matrix quantifying the 'cost' (in a general sense) of moving goods from country i to j. Given the supply vector $\boldsymbol{\mu} \in \mathbb{R}^m$ and the demand vector $\boldsymbol{\nu} \in \mathbb{R}^n$, the optimal transport problem consists in finding a *transport plan*, i.e. a

matrix $\mathbf{T} \in \mathbb{R}_+^{m \times n}$ with entries T_{ij} modelling the total volume (or value) of transport from country i to j, such that the total cost

$$c(\mathbf{T}) = \sum_{i,j} T_{ij} C_{ij} \tag{3}$$

is minimised. In addition, the *marginal constraints*

$$\sum_i T_{ij} = \boldsymbol{\mu}, \ \sum_i T_{ij} = \boldsymbol{\nu} \tag{4}$$

must be satisfied, ensuring that demand and supply are met. It is advantageous to add a *regularisation term* term to the cost, as it ensures existence of a unique solution and significantly improves computational efficiency; the total cost then becomes

$$c_\epsilon(\mathbf{T}) = c(\mathbf{T}) + \epsilon \mathcal{H}(\mathbf{T}), \tag{5}$$

where $\mathcal{H}(\mathbf{T})$ denotes the entropy of $\mathbf{T}$ and $\epsilon > 0$ is a regularisation parameter. It can be shown that the solution will then be of the form

$$\mathbf{T} = \mathbf{\Pi} e^{-\mathbf{C}/\epsilon} \mathbf{\Omega}, \tag{6}$$

where $\mathbf{\Pi}$ and $\mathbf{\Omega}$ are diagonal scaling matrices which ensure that the marginal constraints hold (see Methods).

As described in [20], gravity models can be reformulated as solutions of a regularised OT problem with an appropriate choice of parameters. While OT-based models might appear to suggest a centralised control of flows, its dual formulation admits an alternative, decentralised interpretation (see Methods). Indeed, the dual problem can be interpreted as importers seeking to minimise the cost of purchasing commodities and exporters seeking to maximise their profit. The solution at equilibrium coincides with the solution of the OT problem [21], which in its classic form (3)–(4) is well understood. This is less true for the corresponding *inverse problem* we are interested in, despite its mathematical and practical importance: given a (possibly noisy) observation of $\mathbf{T}$, $\boldsymbol{\mu}$ and $\boldsymbol{\nu}$, this problem consists in inferring the underlying cost $\mathbf{C}$. As shown in [22], maximum likelihood estimation of underlying gravity model parameters can again be reformulated as an inverse optimal transport problem.

The inference methodology presented in this work is a novel deep learning approach to solve the inverse OT problem, based on recent work on neural parameter calibration [23, 24]. We assume no underlying covariate structure, but instead infer a general cost matrix $\mathbf{C}$, parametrized as a deep neural network, directly from data. We train a neural network u to recognise cost matrices from observations of transport

plans for the global food and agricultural trade from 2000–2022 (the '*training data*') by constraining it to satisfy eq. (6). Put simply, this means fitting the mathematical optimal transport equation to the data in such a way that the predicted cost matrices $\mathbf{C}(t)$ reproduce the observations $\mathbf{T}(t)$. The trained neural network then solves the inverse problem

$$\mathbf{C}(t) = u(\mathbf{T}(t)) \tag{7}$$

on the observations. Though its ability to *extrapolate* to new observations depends on the amount of training data, its performance on the training data itself does not. A probability density ρ on the estimates is then naturally obtained by 'pushing' the uncertainty on $\mathbf{T}$ through u, i.e.

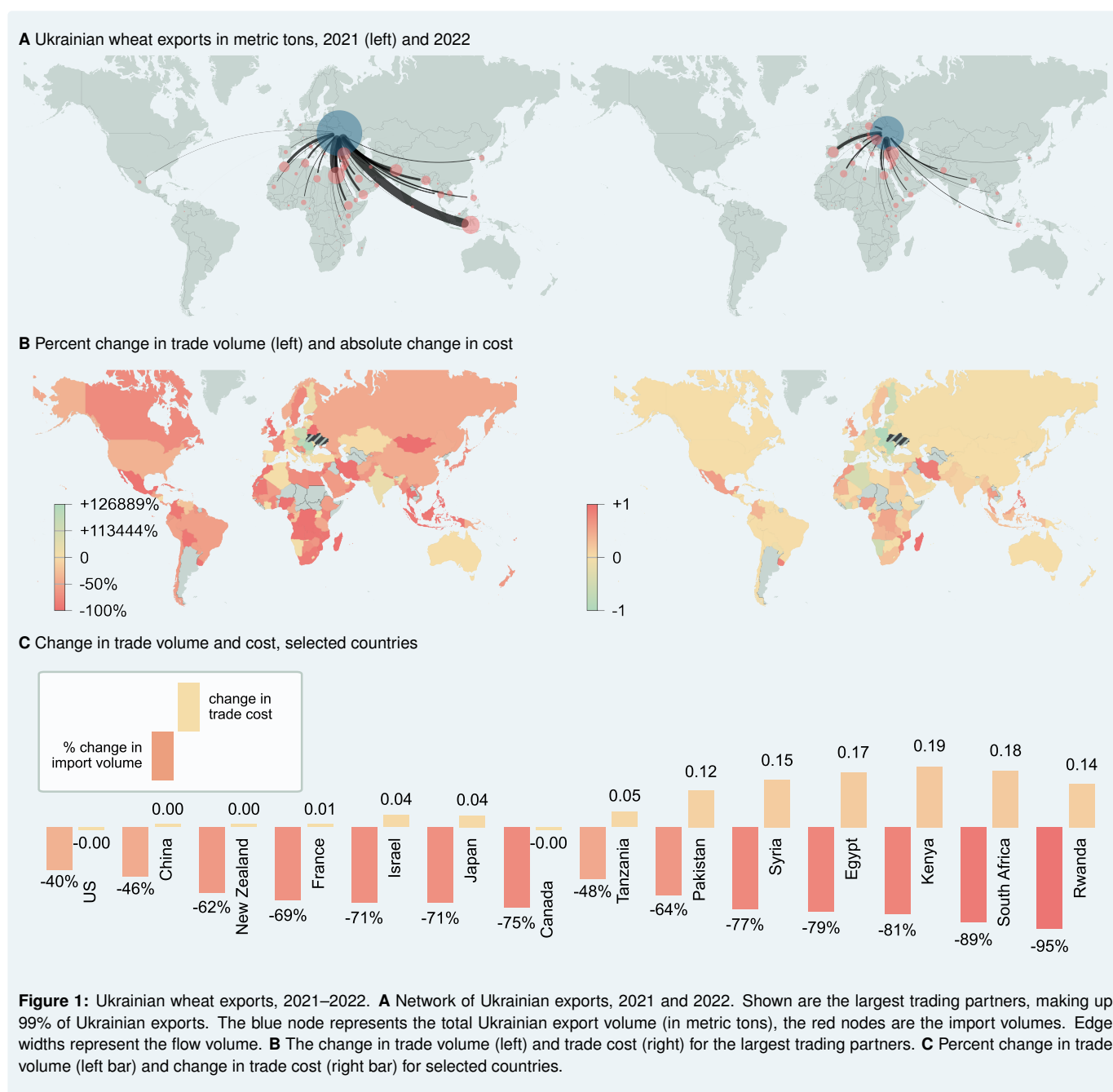$$\rho(\mathbf{C}) = u(\rho(\mathbf{T})) \tag{8}$$

(see Methods). As we demonstrate, this approach produces trade flow estimates that are orders of magnitude more accurate than those of a covariate-based gravity model.

The dataset under consideration was assembled by the Food and Agricultural Organisation of the United Nations (FAO), which provides global trade matrices for over 500 products on its portal[1] [25]. Though extensive, many entries in the trade matrices are missing. Furthermore, the FAO reports two values for each bilateral flow T_{ij}: one reported by the exporter, and one reported by the importer. There is often a considerable discrepancy between the two, due to a multitude of epistemic factors the FAO lists in its accompanying report[2]. The uncertainty on our estimates naturally follows the uncertainty on the FAO data, without presupposing an underlying statistical model.

We apply our method to analyse global commodity flows from 2000–2022, examining the impacts of events, conflicts, trade agreements, and political changes on trade. The cost matrix uncovers economic effects that are not evident in trade volumes or retail prices alone. The article begins with a study of the war in Ukraine's impact on global wheat trade, followed by an analysis of free trade agreements and disputes in the Asia-Pacific, as well as the United Kingdom's 2016 exit from the European Union (Brexit). Finally, we compare our approach to a traditional gravity model, demonstrating its superior performance in both prediction accuracy and uncertainty.

---

[1] https://www.fao.org/faostat/en/#home
[2] https://files-faostat.fao.org/production/TM/TM_e.pdf

A Ukrainian wheat exports in metric tons, 2021 (left) and 2022

B Percent change in trade volume (left) and absolute change in cost

C Change in trade volume and cost, selected countries

Figure 1: Ukrainian wheat exports, 2021–2022. **A** Network of Ukrainian exports, 2021 and 2022. Shown are the largest trading partners, making up 99% of Ukrainian exports. The blue node represents the total Ukrainian export volume (in metric tons), the red nodes are the import volumes. Edge widths represent the flow volume. **B** The change in trade volume (left) and trade cost (right) for the largest trading partners. **C** Percent change in trade volume (left bar) and change in trade cost (right bar) for selected countries.

Results

Case study I: the impact of the Ukrainian war on wheat trade

The Russian Federation's invasion of Ukraine in early 2022 sent shock waves through global food markets [26]. Russia and Ukraine are two of the largest exporters of wheat, together accounting for almost 28% of global wheat exports in 2020. The blockade of trading routes through the Black Sea and the closure or destruction of ports in Mykolaiv and Kherson meant a drop in trade to the overwhelming majority of Ukraine's export destinations, in some cases by as much as 100% (fig. 1A–B). An increase of wheat exports only occurred to Europe, most significantly to Poland, Spain, Slovakia, and Romania, as well as slight increases to Algeria, India,

Figure 2: The same plots as in figure 1 with Russia as the exporting partner.
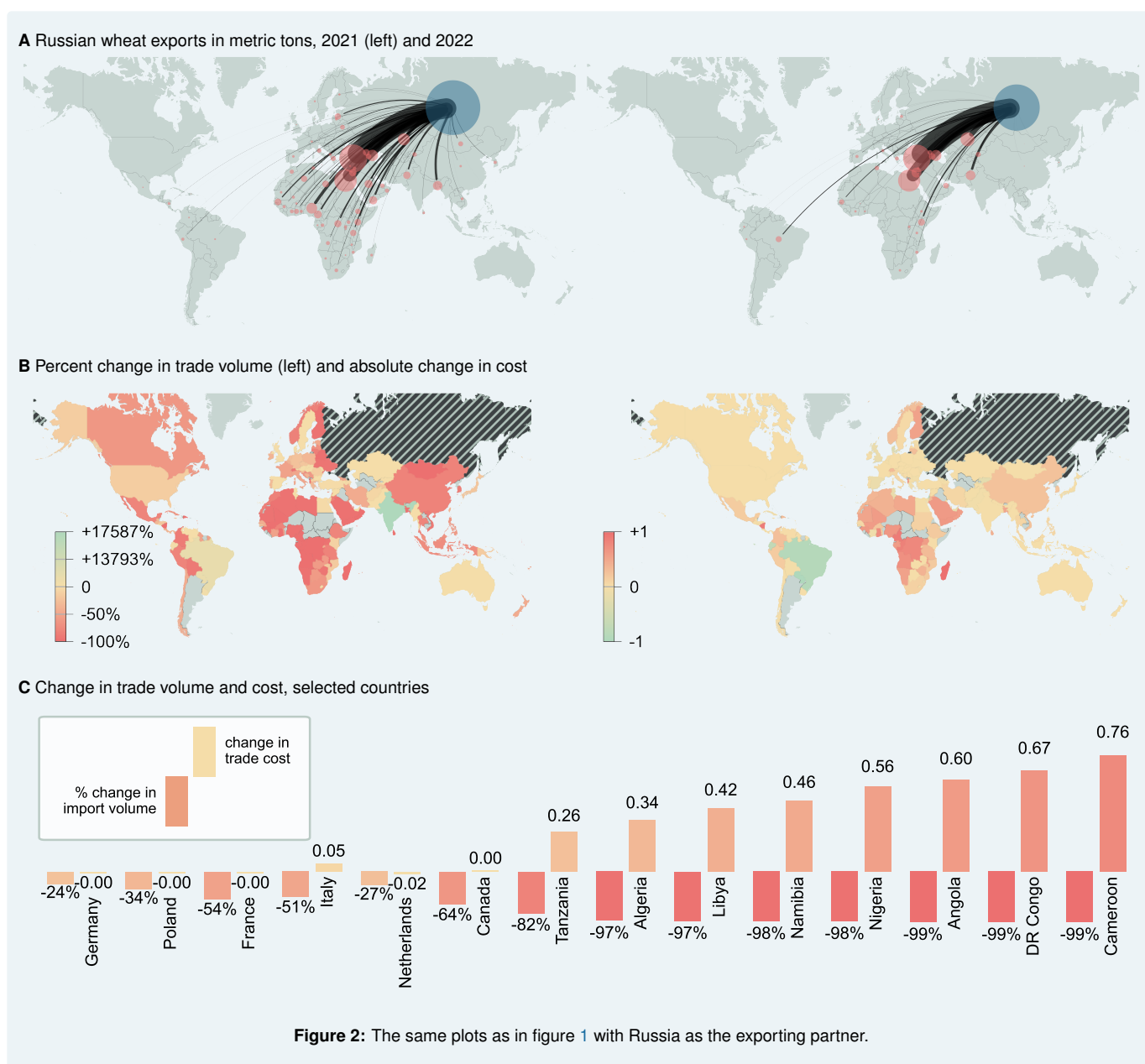
and Türkiye. However, our analysis shows that, although trade shrank across the globe, the accompanying increase in trade costs disproportionately affected the global South, in particular African nations. Of the ten countries with the largest rise in import costs, four are in Africa, and all are in the global South, while of the ten countries with the largest decrease in trade barriers with Ukraine, seven are in Europe. Countries such as Tanzania or Tunisia, while experiencing a similar drop in trade as the US or France, simultaneously saw an increase in their trade costs. Canadian imports fell by

75%, yet trade utility remained constant, while similar drops in Syria or Egypt led to marked increases in trading barriers. European countries saw an average -0.22 point drop in trade barriers with Ukraine, while the African continent saw an average 0.03 point increase. Imports of wheat from Russia also fell globally (fig. 2), again affecting Africa particularly severely. European imports of Russian wheat fell by around 40% with a 0.05 point increase in trade costs; African imports fell by on average 71% with a 0.27 point increase in trade costs. While many European countries saw their imports

of Ukrainian wheat rise, Russian imports fell sharply. Two notable exceptions in our model are the United Kingdom and Netherlands, which saw increases in trading costs with Ukraine of 0.22 and 0.32 respectively. The two largest hubs for Russian wheat, Egypt and Türkiye, saw no change in their import volumes or import barriers. Meanwhile, Iran saw a 0.6 point increase in trade barriers, leading to a 98% percent decline in Ukrainian wheat imports. For Russian wheat, the estimated increase in trade barriers was only 0.05, leading to a drop in imports of 46%. Russian-Iranian trade barriers were thus not markedly affected by the war, despite a drop in trade volumes.

Case study II: Trade in Southeast Asia and Asia-Pacific

A series of free-trade agreements came into effect in Southeast Asia and the Asia-Pacific region in the 2000s and 2010s, significantly among them the China-Australia Free Trade Agreement (ChAFTA) in 2015, the ASEAN-China free trade agreement (ACFTA, gradually entering into force from 2003) and the Comprehensive and Progressive Agreement for Trans-Pacific Partnership (CPTPP) between 11 counties bordering the Pacific Ocean (2018) [27–29]. Together with China's accession to the WTO in 2001 and its rapid economic growth, these trade agreements coincide with some of the largest increases in trade flows in recent history. In figure 3A, we show trade flow of sugar and sugar products from Thailand, Malaysia, and India to China, as well the estimated costs. In our model, the cost of importing sugar from Thailand fell consistently from 2000–2022, following a general trend for ASEAN countries (bottom row, green line) which commenced around 2005. Indian exports, by comparison, remained relatively low up until 2015, when Indian prime minister Narendra Modi visited China, and top officials from both sides agreed to increase bilateral trade to US$100 billion by the end of the year. This visit marked a dramatic shift in Indo-Chinese trade, as exemplified by the huge increase of sugar trade. From 2015–2018, export cost from India dropped sharply by 33%, precipitating a steep increase in trade starting in 2018. By contrast, trade cost from non-ASEAN members has remained constant over the past twenty years (red line, fig. 3A).

The PRC is one of Australia's largest export markets for food and agricultural products. Our analysis shows a precipitous reduction in trade barriers for Australian exports since China's accession to the WTO in 2001 (see fig. 3B), partic-

ularly for beef, wheat, wine, and sugar. Between 2002 and 2010, these commodities saw a 30–80% drop in trade barriers. Our estimates indicate that ChAFTA had little effect on Australian trade costs, since it succeeded a period of deepening ties. Dairy barriers, for instance, had already fallen from 0.35 to 0.14 from 2000 to 2015, thereafter falling a further 0.03 points until 2020. Wine exports too saw their largest reductions in trade barriers between 2000 and 2010, only experiencing a 0.04 drop from 2015 to 2018 compared to the 0.59 point reduction from 2000–2015.

In January 2018, the Trump administration started imposing import tariffs on goods primarily from China. In response, the Chinese government increased tariffs on a variety of products, including agricultural imports. The largest agricultural export from the US to China, soya beans, were hit with a 25% import tariff [30]. Meanwhile, political tensions between China and Australia caused Beijing to introduce high anti-dumping tariffs on Australian exports such as barley (80.5%) and wine (206%), starting in 2020 [31]. Wine trade had previously been tariff-free since the signing of ChAFTA in 2015. Our analysis provides an estimate of the change in the ease of trading these measures induced (figs. 3B and 4). Australian beef, wine and barley imports all experience large increases in cost, following the implosion of trade volumes. Australia was able to divert some of its excess barley supply to Saudi Arabia, which saw a decrease in trade barriers of over 0.5 points between 2019 and 2022 (fig. 4C). Trade volumes to Vietnam also increased from 200,000 to 800,000 metric tons, though trade costs remained approximately constant. Meanwhile, after 2020 China doubled its barley imports from Canada and France. We found that import barriers from both countries were reduced slightly in 2021, though they increased again in the year after.

Case study III: Brexit

In 2016, the United Kingdom voted to leave the European Union, officially exiting the common market and customs union on December 31, 2020. This case study examines the impact of Brexit on British import patterns by comparing vegetable and wine imports from mainland Europe to both the United Kingdom and the Republic of Ireland (ROI), which remains part of the Eurozone and the common market. While both island nations naturally source the majority of their fresh produce from mainland Europe, their trading patterns have evolved in markedly different ways. Imports of lettuce from Europe generally fell for the UK, accompanied
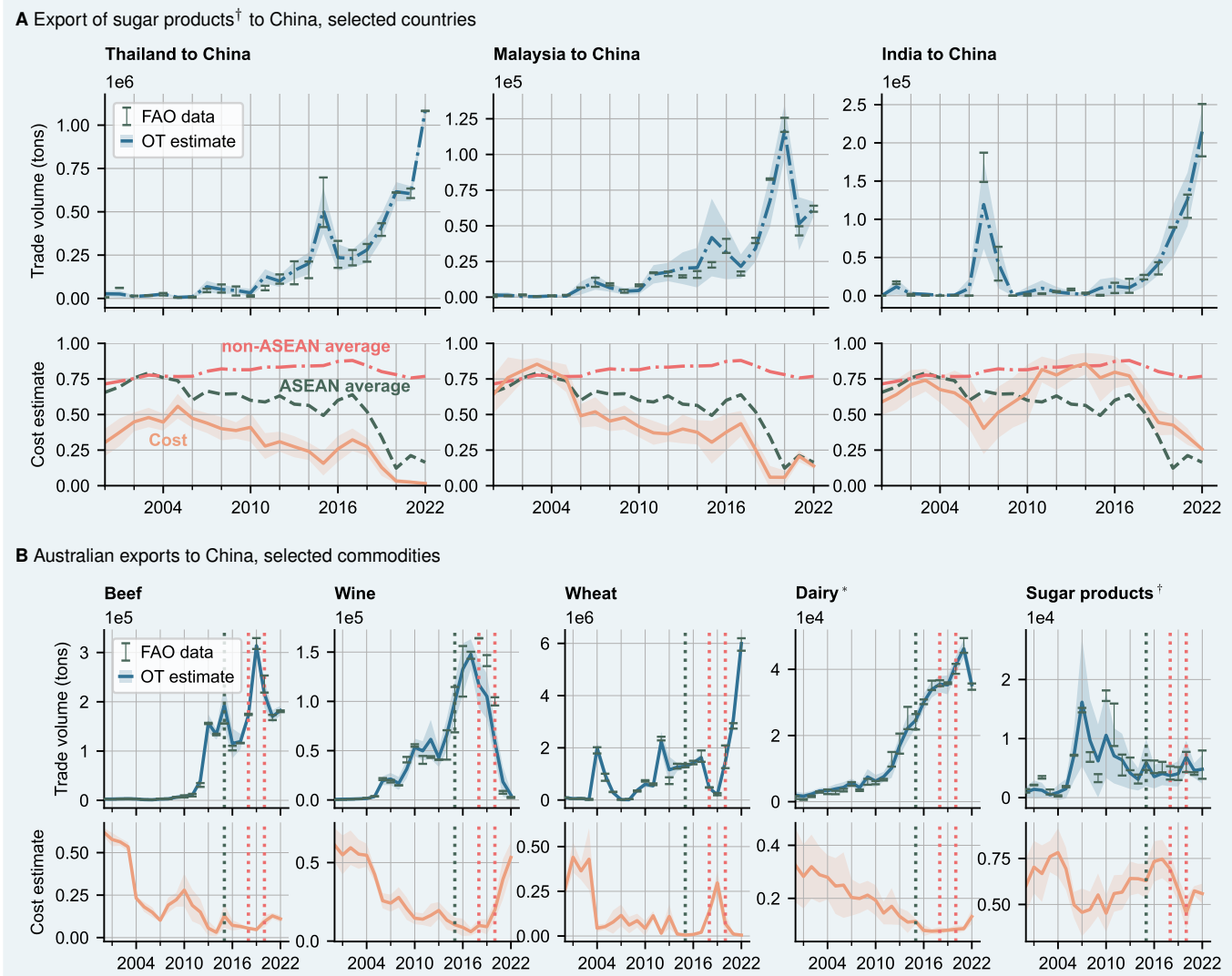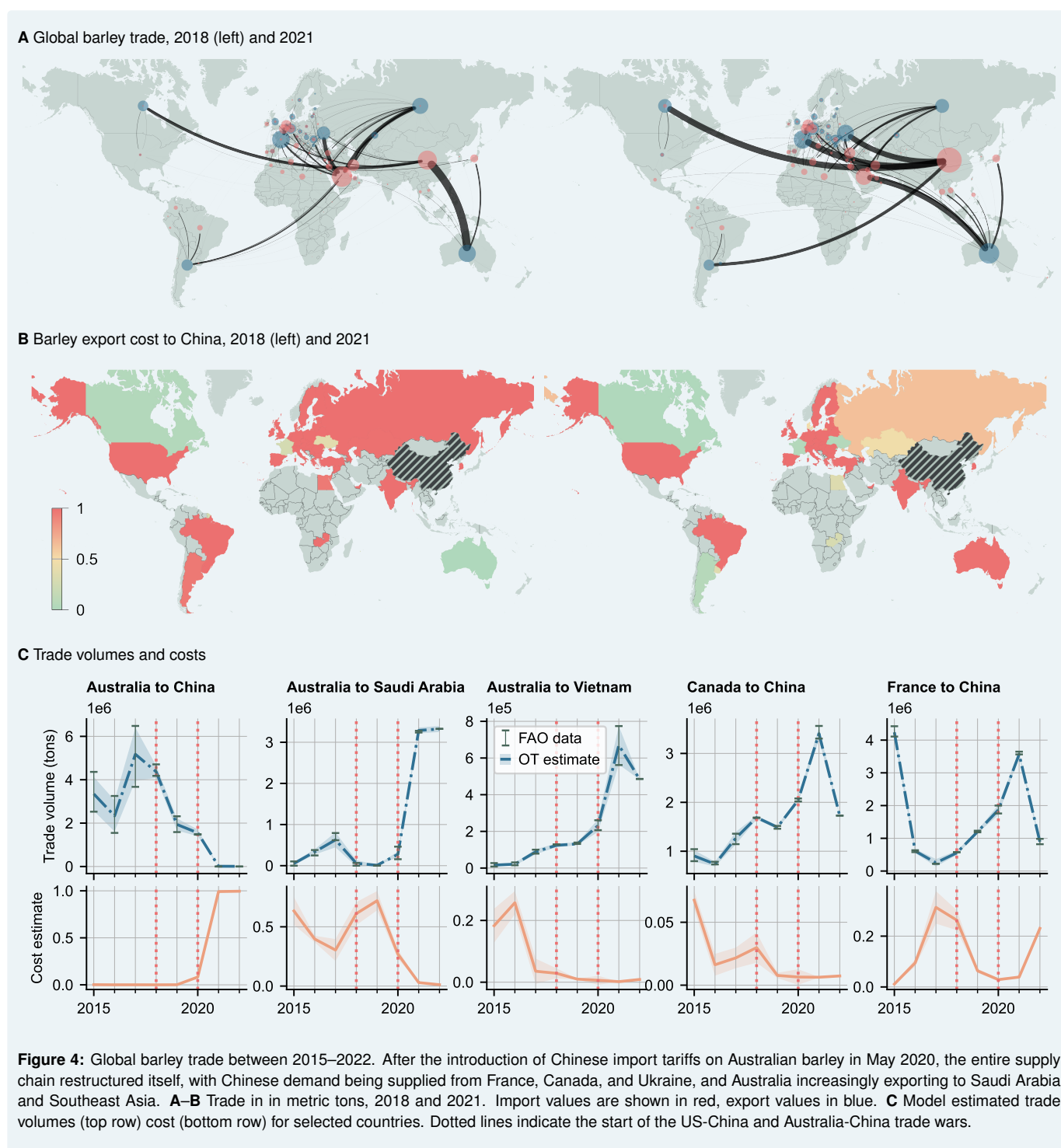
A Export of sugar products[†] to China, selected countries

B Australian exports to China, selected commodities

Figure 3: Trade with China. **A** Export of sugar products to China. Top row: estimated trade volume (light blue) in metric tons, as well as the reported values. Bottom row: estimated cost, together with the ASEAN and non-ASEAN averages. **B** Australian exports to China, selected commodities. Top row: model estimated flow and FAO data; bottom row: estimated cost. Indicated are the signing of ChAFTA (2015, green dotted line) as well as the start of the US-China and Australia-China trade disputes (2018 and 2020, red dotted lines). Errorbands indicate one standard deviation.

[†] Sugar products comprise: sugar, refined sugar, syrups, fructose, sugar confectionery. [*] Dairy products comprise: butter, skim milk of cows, cheese, other dairy products.

by a rise in import cost: −44% trade volume and +0.11 in import costs from the Netherlands, the largest exporter of lettuce and chicory to the UK, as well as a −21% drop in trade from Spain, though with no change in import cost. Ireland increased its imports of lettuce and other greens from the Netherlands, Spain, Italy, and Portugal, accompanied by a general decrease in trading costs. In the case of the Netherlands, Ireland saw a consistent reduction in vegetable trade costs, unlike the United Kingdom. It is interesting to note that the United Kingdom significantly increased its imports of vegetables from Morocco, accompanied by a precipitous drop in trade costs, indicating a facilitation of trade between the two countries in the wake of Brexit. This is not true for the ROI: though it increased its imports of Moroccan tomatoes by nearly twice as much as the UK, Irish trade costs still fell by less than for the UK.

A more clear-cut trend emerges in the wine trade (fig. 6B): here, the UK was consistently affected more negatively

Figure 4: Global barley trade between 2015–2022. After the introduction of Chinese import tariffs on Australian barley in May 2020, the entire supply chain restructured itself, with Chinese demand being supplied from France, Canada, and Ukraine, and Australia increasingly exporting to Saudi Arabia and Southeast Asia. **A–B** Trade in in metric tons, 2018 and 2021. Import values are shown in red, export values in blue. **C** Model estimated trade volumes (top row) cost (bottom row) for selected countries. Dotted lines indicate the start of the US-China and Australia-China trade wars.

than the Republic of Ireland: British import costs from all eight countries considered rose by considerably more than those of the ROI. An 11% drop in Spanish wine import was accompanied by a 0.09 point increase in trading costs, while a −8% change in Irish imports was nonetheless accompanied by a 0.01 point decrease in costs. Portugese wine imports to the UK rose by 24%, notwithstanding a 0.07 increase in trade costs. The picture is unchanged for South African,
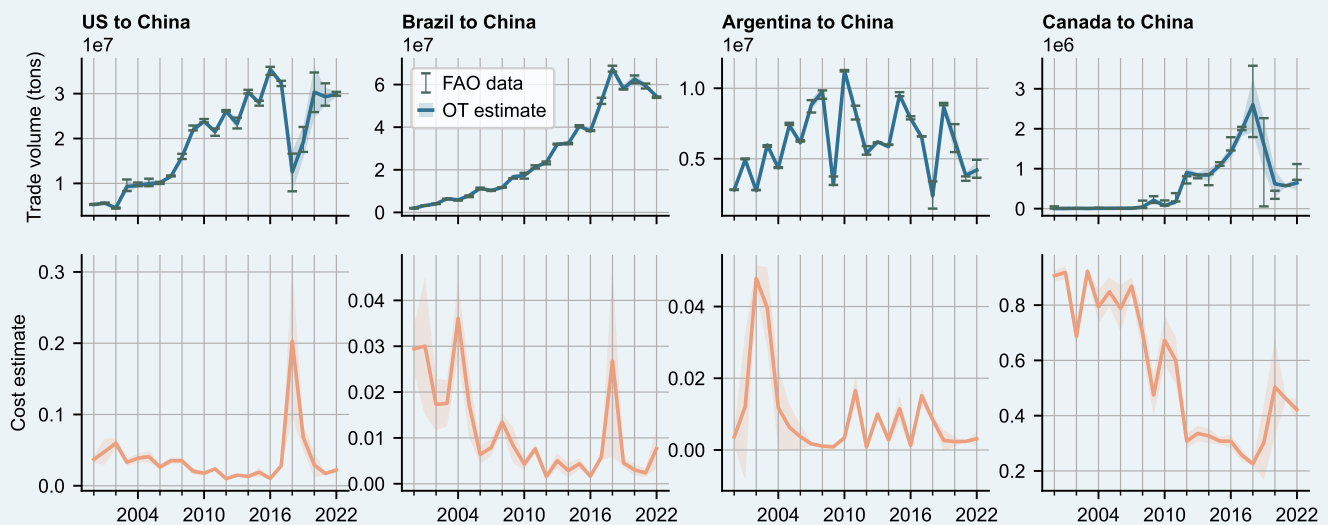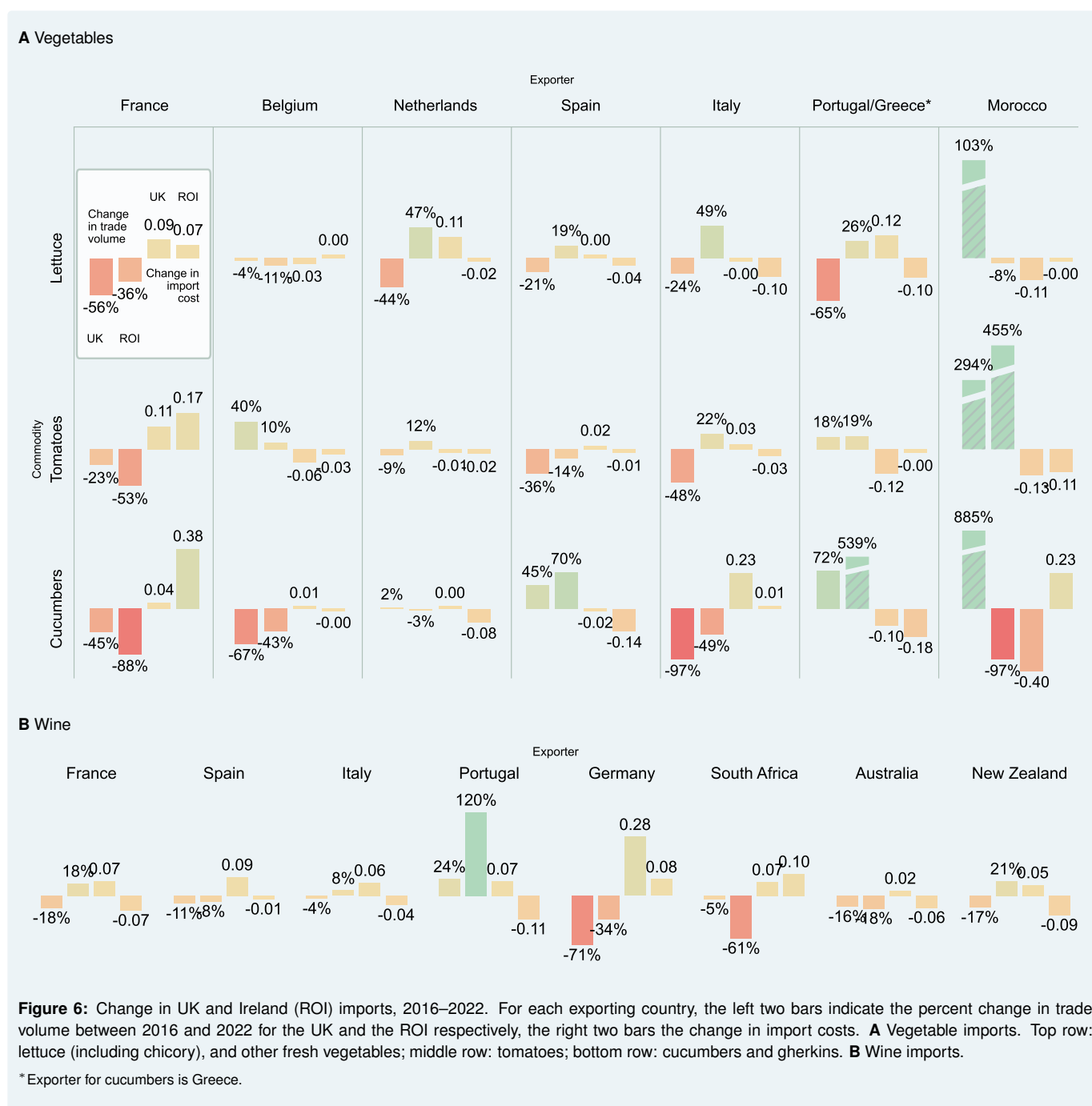
A Global soya bean trade, 2016 (left) and 2018
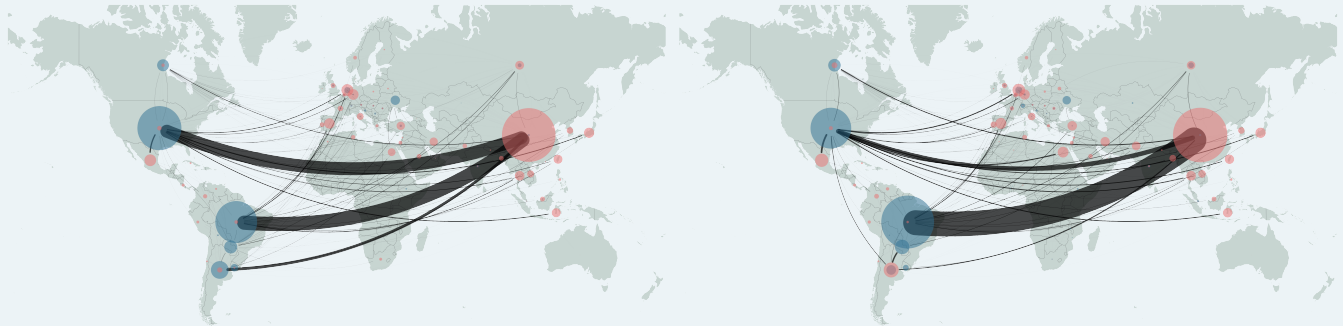
B Yield
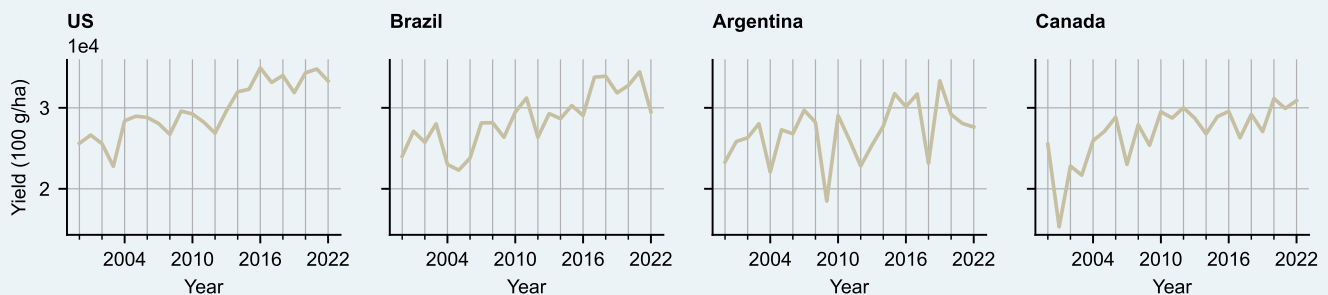
C Trade volumes and utilities

Figure 5: Global soya bean trade. **A** In 2018, the Chinese government raised import tariffs on American soya beans in a retaliatory action against US trade restrictions. The shortfall was met by imports from Brazil. **B** Soya bean yield in 100 g/hectare. Argentina in 2018 experience a major drop in yields, leading to an increase in exports from the US **C** Predicted trade volumes in metric tons (top row) and predicted cost (bottom row).

Australian, and New Zealand imports. The EU maintains free trade or regulatory agreements removing wine import duties with the former two [32, 33]. When the UK left the European Union, wine from Australia entered at the UK Global Tariff rate, which in mid-2023 was eliminated under the Australia-United Kingdom FTA [34]. South African wines, by contrast, continued to be imported to the UK tariff-free post-Brexit [35]. Yet here too, the United King-

A Vegetables

B Wine

Figure 6: Change in UK and Ireland (ROI) imports, 2016–2022. For each exporting country, the left two bars indicate the percent change in trade volume between 2016 and 2022 for the UK and the ROI respectively, the right two bars the change in import costs. **A** Vegetable imports. Top row: lettuce (including chicory), and other fresh vegetables; middle row: tomatoes; bottom row: cucumbers and gherkins. **B** Wine imports.

*Exporter for cucumbers is Greece.

dom's 5% decrease in imports was driven by a 0.07 increase in trading costs; Ireland, by contrast, imported an estimated 61% less wine, driven by a comparable 0.1 point increase in trading costs.

Comparison with Gravity model

Lastly, we compare the performance of our method with a standard gravity model [11, 36–38], as specified in equations (1)–(2). The covariates include geographic distance, shared borders, colonial ties, common language, regional trade agreements, tariffs, and importer/exporter fixed effects to
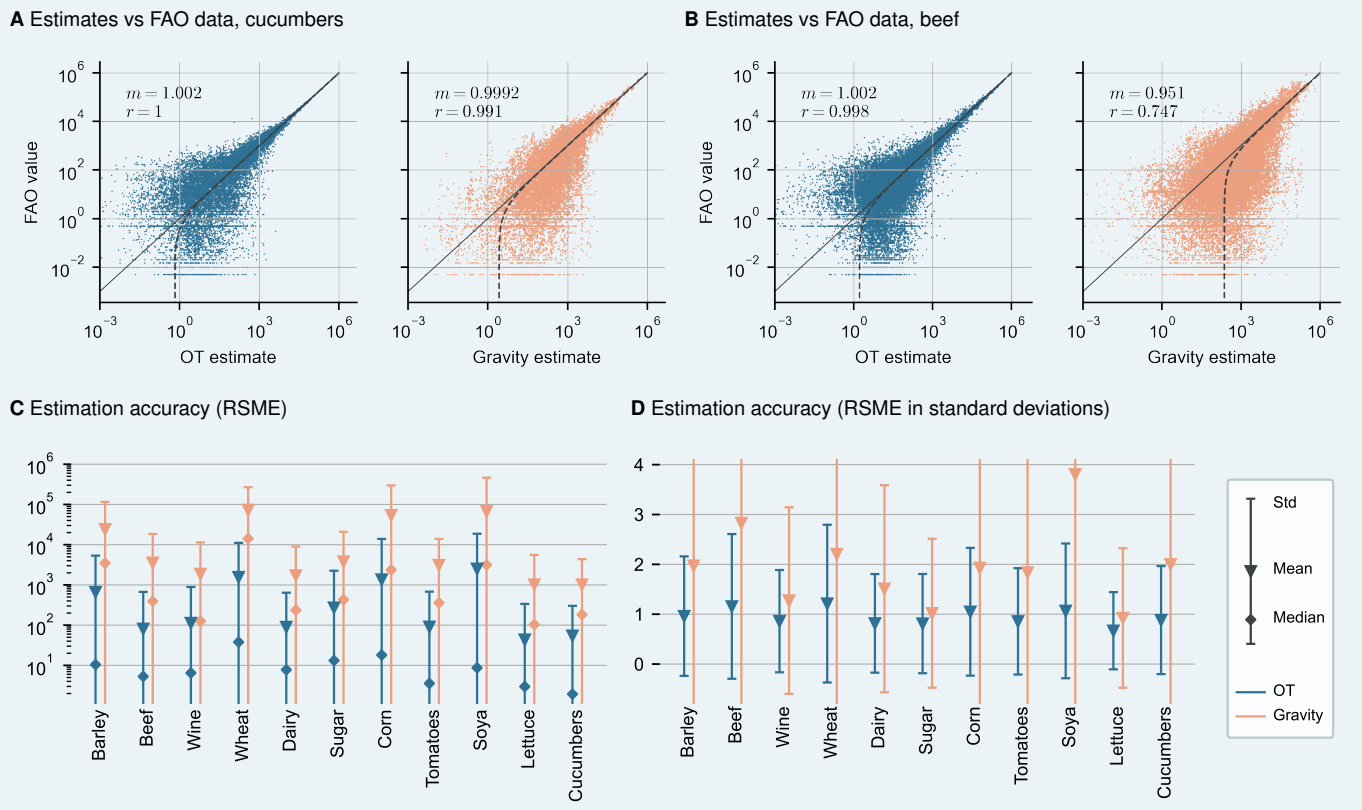
Figure 7: Comparison with gravity model. **A–B** Comparison plot of the OT and gravity estimates (x-axis) versus the true data (y-axis) on two selected commodities. Also shown is a linear fit (dotted line), its estimated slope m, the Pearson coefficient of the fit r, and the line $y = x$ (solid line). See fig. S1 in the appendix for an overview of all commodities. **C–D** Comparison of the RMSE accuracies of the estimated transport volumes of the OT approach (blue) and the gravity model (orange). Values are averaged over all countries and years, with the errorbars showing one standard deviation from the mean (triangular marker). Also shown are the median values (diamond markers). Shown are the RMSE (left) and the RMSE in units of the standard deviation on the true data (right).

account for multilateral resistance (see Supplementary Information for details). We estimate the coefficients using Poisson Pseudo Maximum Likelihood estimation and compare the accuracy of the estimated transport plans **T**. Figures 7A–B show scatter plots of the OT (blue) and gravity (orange) estimates against the FAO data. For all commodities studied, a linear fit through the OT estimates yields a near-perfect slope of $m = 1$ with a Pearson coefficient close to 1, perfectly fitting the tail end of the distribution. In contrast, the gravity model's performance is much more volatile, with linear fits ranging from a Pearson coefficient of between 0.998 (best) to 0.747 (worst) (see also Supplementary Information). Due to model misspecification, the fits to the tails of the distributions are generally significantly poorer. Consequently, figure 7C shows that the OT approach significantly outperforms the gravity model in terms of RMSE, often by two to three

orders of magnitude. Figure 7D illustrates that OT estimates typically fall within one standard deviation of the data uncertainty, whereas gravity estimates tend to range from one to two, at times even three to four standard deviations. The gravity model also exhibits much higher variance in accuracy compared to OT.

Discussion

This paper introduces a novel and versatile approach for identifying the drivers and barriers of global commodity trades. Using optimal transport theory, we are able to obtain a cost structure that is more expressive than a covariate-based gravity approach. Our estimates are thus orders of magnitude more accurate than the current state of the art, while providing consistent accuracy across datasets. The optimal transport ap-

proach models trade networks as a dynamical, interconnected system, allowing to capture complex rearrangements and network response dynamics to e.g. trade wars, conflicts, or shifts in political relations. By contrast, the covariate-based gravity approach fits each node in the network individually without taking interaction effects into account. Though the current work looks only at global agrifood markets, the methodology proposed is general and applicable to commodity flows, financial markets, or banking networks [39]. Beyond economics, the optimal transport approach also relates e.g. to global migration flows, which can be estimated from stock data [40,41].

Method

Entropy-regularised Optimal Transport

In OT one wishes to find the optimal flow of mass from a source distribution to a target distribution, while minimising an overall transport cost. This abstract problem has a wide range of applications in economics, logistics, image restoration, transport systems, or urban structure [21, 42, 43].

Consider an m-dimensional space X, an n-dimensional space Y, and furthermore a non-negative measure $\mathbf{C}$ on $X \times Y$. The entries of $\mathbf{C}$ correspond to the cost of transporting mass from one location in X to a target in Y. Given two probability measures $\boldsymbol{\mu} \in P(X)$ and $\boldsymbol{\nu} \in P(Y)$ (the supply and demand), the OT problem consists in finding a *transport plan* $\mathbf{T}$ minimising the overall cost eq. (3). The transport plan $\mathbf{T}$ must also satisfy the *marginal constraints*

$$\sum_j T_{ij} = \boldsymbol{\mu} \text{ and } \sum_i T_{ij} = \boldsymbol{\nu}. \quad (9)$$

In practice one usually solves the *entropy regularised* OT formulation, which can be solved much more efficiently [44]; here, an additional term is added to the objective:

$$\min_{\mathbf{T}} \sum_{ij} C_{ij} T_{ij} + \epsilon \sum_{ij} T_{ij} \left(\log T_{ij} - 1 \right), \quad (10)$$

where $\epsilon > 0$ is a positive regularisation parameter. This regularisation prevents monopolisation, i.e. demand being supplied from only a few sources.

This constrained optimisation problem eq. (10) can be solved by considering the Lagrangian

$$\mathcal{L} = \sum_{ij} T_{ij} C_{ij} + \langle \boldsymbol{\lambda}, \sum_j T_{ij} - \boldsymbol{\mu} \rangle + \langle \boldsymbol{\eta}, \sum_i T_{ij} - \boldsymbol{\nu} \rangle$$
$$+ \epsilon \sum_{ij} T_{ij} \left(\log T_{ij} - 1 \right), \quad (11)$$

with $\boldsymbol{\lambda} \in \mathbb{R}^m$ and $\boldsymbol{\eta} \in \mathbb{R}^n$ Lagrangian multipliers. Minimising $\mathcal{L}$ with respect to $\mathbf{T}$ gives the solution

$$T_{ij} = e^{-\lambda_i/\epsilon} e^{-C_{ij}/\epsilon} e^{-\eta_j/\epsilon} \quad (12)$$

or

$$\mathbf{T} = \mathbf{\Pi} e^{-\mathbf{C}/\epsilon} \mathbf{\Omega}, \quad (13)$$

where $\mathbf{\Pi} = \mathrm{diag}(e^{-\lambda_1/\epsilon}, \cdots, e^{-\lambda_m/\epsilon}) \in \mathbb{R}^{m \times m}$ and $\mathbf{\Omega} = \mathrm{diag}(e^{-\eta_1/\epsilon}, \cdots, e^{-\eta_n/\epsilon}) \in \mathbb{R}^{n \times n}$ are diagonal matrices of Lagrangian multipliers.

Finding $\mathbf{\Pi}$ and $\mathbf{\Omega}$ is achieved through an iterative procedure that is variously called *Iterative Proportionate Procedural Fitting* (IPFP), *RAS*, or *Sinkhorn's algorithm* [44–46]. Define $\mathbf{M} = e^{-\mathbf{C}/\epsilon}$; then, given an initial guess $\mathbf{\Pi}^0$, we update $\mathbf{\Omega}$ to satisfy the first marginal constraint eq. (9)

$$\mathbf{\Omega} \mathbf{M}^\top \mathbf{\Pi}^0 = \boldsymbol{\nu}. \quad (14)$$

Solving for $\mathbf{\Omega}$ gives

$$\mathbf{\Omega}^0 = \frac{\boldsymbol{\nu}}{\mathbf{M}^\top \mathbf{\Pi}^0} \quad (15)$$

where the division is understood element-wise. Similarly, we obtain the next update for $\mathbf{\Pi}$ as

$$\mathbf{\Pi}^1 = \frac{\boldsymbol{\mu}}{\mathbf{M} \mathbf{\Omega}^0}, \quad (16)$$

and so on. The algorithm can thus be summarised as follows:

Algorithm 1 Sinkhorn's Algorithm

1: **Inputs:**
    $\mathbf{M}$ (Exponential of cost matrix)
    $\boldsymbol{\mu}, \boldsymbol{\nu}$ (marginals)
2: Initialise the first Lagrangian multiplier $\mathbf{\Pi}^0$
3: **for** n iterations **do**
4:     $\mathbf{\Omega}^{i+1} \leftarrow \dfrac{\boldsymbol{\nu}}{\mathbf{M} \mathbf{\Pi}^i}$
5:     $\mathbf{\Pi}^{i+1} \leftarrow \dfrac{\boldsymbol{\mu}}{\mathbf{M}^\top \mathbf{\Omega}^{i+1}}$
6: **end for**

Under certain conditions, convergence of the algorithm to a unique solution is guaranteed [47, 48]. Note the important fact that the solution $\mathbf{T}$ is invariant under scaling of the cost matrix, since the Lagrangian multipliers absorb the scaling; the transport plan thus does not depend on *absolute* cost values, only on their relative proportions.

The classic OT problem eq. (6) can be interpreted as the central's planners problem of finding the optimal assignment/matching of supplies and demands. The dual OT problem is given by

$$\max_{\boldsymbol{f},\boldsymbol{g}}\langle\boldsymbol{f},\boldsymbol{\mu}\rangle + \langle\boldsymbol{g},\boldsymbol{\nu}\rangle \qquad (17)$$

such that $\boldsymbol{f}\in\mathbb{R}^n$ and $\boldsymbol{g}\in\mathbb{R}^m$ satisfy

$$\boldsymbol{f}\oplus\boldsymbol{g}\leq\boldsymbol{C} \qquad (18)$$

where $\boldsymbol{f}\oplus\boldsymbol{g} = \boldsymbol{f}\mathbf{1}_m^T + \boldsymbol{g}\mathbf{1}_n^T$. Here $\boldsymbol{f}$ and $\boldsymbol{g}$ can be interpreted as the minimal cost of picking up and dropping off a good at locations respectively. The central planner problem of finding the best plan $\mathbf{T}$ is therefore split into determining the optimal cost of collecting and delivering goods. The constraint (18) ensures optimality. If $f_i + g_j > C_{ij}$, that is the cost of picking up a good at location i and dropping it off at location j is larger than the transportation cost, it can not be optimal.

Neural Inverse Optimal Transport

To infer the cost matrix function $\mathbf{C}(t)$ from a dataset of transport plan observations $\mathbf{T}(t)$, we build on the neural parameter estimation method first introduced in [23] and subsequently expanded upon [24]. We wish to train a neural network u to solve the inverse OT problem $\mathbf{C}(t) = u(\mathbf{T}(t))$. We do so by constructing a loss function that differentiates through the optimal transport equations, i.e.

$$J = \|\hat{\mathbf{T}}(\hat{\mathbf{C}}) - \mathbf{T}\|_2^2 + \|\sum_j C_{ij} - 1\|_1. \qquad (19)$$

Here, $\hat{\mathbf{T}}(\hat{\mathbf{C}})$ is the estimated transport plan obtained by solving Sinkhorn's algorithm alg. [1]. The second summand together with the restriction that $0 \leq C_{ij} \leq 1$ is necessary to fix the cost matrix since the OT problem is in general invariant under affine transformations of $\mathbf{C}$. Using this approach, the quality of the prediction does not depend on the number of datasets used to train the neural network, since we are not performing regression, but rather fitting a mathematical model (or a set of parameters) to data. The data is processed in batches, and a gradient descent step performed on the neural network parameters after each batch. The loss is only calculated for links with trade flow > 0.

As mentioned, the FAO dataset contains two values for each entry T_{ij}: one reported by the exporter, and one by the importer. Let $\mathbf{T}^{\mathrm{E}}$ by the transport plan where all entries are those reported by the exporters, and $\mathbf{T}^{\mathrm{I}}$ those where all are reported by the importers. The *training data*—i.e., the data we use to train the function u—consists of only these two transport plans for each year: $\{\mathbf{T}^{\mathrm{E}}(t), \mathbf{T}^{\mathrm{I}}(t)\}$, giving a total training set size of $2 \times L$, where $L = 23$ are the number of observation points. A hyperparameter sweep showed that using a deep neural network with 5 layers, 60 nodes per layer, and hyperbolic tangent activation functions on all layers but the last, where we use a sigmoid, gives best results. Using a sigmoid activation function on the last layer ensures $0 \leq C_{ij} \leq 1$. We use the Adam optimizer [49] to train the neural network. We pool all FAO trade matrices to only contain those countries that account for 99% of import and export volumes, subsuming all other countries in an 'Other' category (thereby ensuring that no flow is lost). Missing entries in the training data are masked and do not contribute to the loss function.

Uncertainty quantification on the estimated cost matrix $\hat{\mathbf{C}}$ is obtained by passing random samples of $\mathbf{T}$ through the trained neural network u. These samples are obtained by selecting either T_{ij}^{E} or T_{ij}^{I} uniformly at random for each entry of the transport plan, and passing this sample through the neural network. Repeating this n times gives n samples of $\mathbf{C}$, and inserting each estimate of $\mathbf{C}$ into Sinkhorn's algorithm gives n estimated transport plans $\hat{\mathbf{T}}$. We generate $n = 1000$ samples for each year.

Code and data availability

All code and data is available at https://github.com/ThGaskin/inverse-optimal-transport. Instructions for running the model are given in the README.

Acknowledgements

References

[1] S Friel, A Schram, B Townsend, The nexus between international trade, food systems, malnutrition and climate change. *Nature Food* **1**, 51–58 (2020).

[2] A Wood, et al., Reframing the local–global food systems debate through a resilience lens. *Nature Food* **4**, 22–29 (2023).

[3] Grain Industry Association of Western Australia, China barley antidumping and counterveilling tariffs (2020).

[4] Federal Reserve Bank of St. Louis, Global price of barley (2024).

[5] J Eaton, S Kortum, Technology, Geography, and Trade. *Econometrica* **70**, 1741–1779 (2002).

[6] JE Anderson, E van Wincoop, Gravity with Gravitas: A Solution to the Border Puzzle. *American Economic Review* **93**, 170–192 (2003).

[7] C Arkolakis, A Costinot, A Rodríguez-Clare, New Trade Models, Same Old Gains? *American Economic Review* **102**, 94–130 (2012).

[8] T Allen, C Arkolakis, Y Takahashi, Universal Gravity, (National Bureau of Economic Research, Inc), NBER Working Papers 20787 (2014).

[9] Y Yotov, Gravity at sixty: The workhorse model of trade (2022).

[10] R Dekle, J Eaton, S Kortum, Global Rebalancing with Gravity: Measuring the Burden of Adjustment, (National Bureau of Economic Research, Inc), NBER Working Papers 13846 (2008).

[11] YV Yotov, R Piermartini, JA Monteiro, M Larch, *An Advanced Guide to Trade Policy Analysis*. (United Nations), (2017).

[12] A Olper, V Raimondi, Patterns and determinants of international trade costs in the food industry. *Journal of Agricultural Economics* **60**, 273–297 (2009).

[13] R Sarker, S Jayasinghe, Regional trade agreements and trade in agri-food products: evidence for the european union from gravity modeling using disaggregated data. *Agricultural Economics* **37**, 93–104 (2007).

[14] I Mujahid, M Kalkuhl, Do trade agreements increase food trade? *The World Economy* **39**, 1812–1833 (2016).

[15] V Raimondi, A Olper, Trade elasticity, gravity and trade liberalisation: Evidence from the food industry. *Journal of Agricultural Economics* **62**, 525–550 (2011).

[16] G Philippidis, H Resano-Ezcaray, AI Sanjuán-López, Capturing zero-trade values in gravity equations of trade: an analysis of protectionism in agro-food sectors. *Agricultural Economics* **44**, 141–159 (2013).

[17] H Breinlich, D Novy, JMC Santos Silva, Trade, Gravity, and Aggregation. *The Review of Economics and Statistics* **106**, 1418–1426 (2024).

[18] L Capoani, Review of the gravity model: origins and critical analysis of its theoretical development. *SN Business & Economics* **3**, 1–43 (2023).

[19] C Villani, *Topics in optimal transportation*. (American Mathematical Soc.) Vol. 58, (2021).

[20] A Wilson, A statistical theory of spatial distribution models. *Transportation Research* **1**, 253–269 (1967).

[21] A Galichon, *Optimal Transport Methods in Economics*. (Princeton University Press), 1 edition, (2016).

[22] JS Silva, S Tenreyro, The log of gravity. *The Review of Economics and statistics* **88**, 641–658 (2006).

[23] T Gaskin, GA Pavliotis, M Girolami, Neural parameter calibration for large-scale multi-agent models. *PNAS* **120** (2023).

[24] T Gaskin, GA Pavliotis, M Girolami, Inferring networks from time series: A neural approach. *PNAS Nexus* **3**, 63 (2024).

[25] Food and Agriculture Organization of the United Nations, FAOSTAT statistical database (c1997-).

[26] M Laber, P Klimek, M Bruckner, L Yang, S Thurner, Shock propagation from the Russia–Ukraine conflict on international multilayer food production network determines global food availability. *Nature Food* **4**, 508–517 (2023).

[27] Australian Government, Department of Foreign Affairs and Trade, China–Australia Free Trade Agreement (2017).

[28] ASEAN-China Free Trade Area Business Portal, ASEAN–China Free Trade Area (2016).

[29] Australian Government, Department of Foreign Affairs and Trade, Comprehensive and Progressive Agreement for Trans-Pacific Partnership (CPTPP) (2018).

[30] T Biesheuvel, Bloomberg: As China Fires Back in Trade War, Here Are the Winners And Losers (https://www.bloomberg.com/news/articles/2018-04-04/as-china-fires-back-in-trade-war-here-are-the-winners-and-losers) (2018) [Accessed 07-09-2024].

[31] T Biesheuvel, ABC News: China's list of sanctions and tariffs on Australian trade is growing. Here's what has been hit so far (https://www.abc.net.au/news/2020-12-17/australian-trade-tension-sanctions-china-growing-commodities/12984218) (2020) [Accessed 07-09-2024].

[32] European Commission, EU-SADC Economic Partnership Agreement (EPA) (2016).

[33] Winemakers Federation of Australia, Submission on Australia-European Union Free Trade Agreement (2016).

[34] Department of Agriculture, Fisheries and Forestry of Australia, Analysis – Opportunities for Australian wine exports to the UK (2023).

[35] VINPRO, SA wine exporters still benefit post-Brexit (2020).

[36] M Conte, P Cotterlaz, T Mayer, The CEPII Gravity Database, (CEPII research center), Working Papers 2022-05 (2022).

[37] United Nations Conference on Trade and Development, Unctad trains database (2020).

[38] World Trade Organisation, Wto stats (2024).

[39] K Giesecke, G Schwenkler, JA Sirignano, Inference for large financial systems. *Math. Finance* **30**, 3–46 (2020).

[40] JJ Azose, AE Raftery, Estimation of emigration, return migration, and transit migration between all pairs of countries. *Proceedings of the National Academy of Sciences* **116**, 116–122 (2018).

[41] F Willekens, Modeling approaches to the indirect estimation of migration flows: From entropy to EM. *Mathematical Population Studies* **7**, 239–278 (1999) PMID: 12295226.

[42] F Santambrogio, Optimal transport for applied mathematicians. *Birkhäuser, NY* **55**, 94 (2015).

[43] G Peyré, M Cuturi, , et al., Computational optimal transport: With applications to data science. *Foundations and Trends® in Machine Learning* **11**, 355–607 (2019).

[44] M Cuturi, Sinkhorn distances: Lightspeed computation of optimal transport. *Advances in neural information processing systems* **26** (2013).

[45] WE Deming, FF Stephan, On a Least Squares Adjustment of a Sampled Frequency Table When the Expected Marginal Totals are Known. *The Annals of Mathematical Statistics* **11**, 427–444 (1940).

[46] M Idel, A review of matrix scaling and Sinkhorn's normal form for matrices and positive maps (2016).

[47] R Sinkhorn, A Relationship Between Arbitrary Positive Matrices and Doubly Stochastic Matrices. *The Annals of Mathematical Statistics* **35**, 876–879 (1964).

[48] L Rueschendorf, Convergence of the Iterative Proportional Fitting Procedure. *Annals of Statistics* **23** (1995).

[49] DP Kingma, J Ba, Adam: A Method for Stochastic Optimization. *arXiv* **1412.6980 [cs.LG]** (2014).

Supporting Information

Comparison with Gravity model

Coefficient	Barley	Beef	Wine	Wheat	Dairy products[*]	Sugar products[†]	Corn	Tomatoes
λ_1	0.0771	0.107	0.122	0.051	0.0905	0.0413	0.0703	0.0794
λ_2	0.0296	0.00551	0.0598	0.0691	0.107	0.0689	0.0617	0.084
λ_3	-1.88	-1.57	-1.17	-2.02	-1.51	-1.92	-2.19	-2.23
λ_4	-2.04	-0.758	-1.26	-1.43	-1.23	-0.62	-1.23	-0.881
λ_5	-0.69	0.152	0.979	-0.115	0.562	1.03	0.111	0.0681
λ_6	-0.254	0.0632	0.972	0.0436	0.694	0.525	-0.298	0.987
λ_7	-0.312	0.606	0.409	-0.0619	0.619	0.506	0.192	0.953
λ_8	0.496	0.182	0.211	0.459	0.198	0.322	0.339	0.182
λ_9	0.495	0.194	0.196	0.387	0.393	0.333	0.395	0.26

Coefficient	Soya beans	Vegetables	Cucumbers and gherkins
λ_1	0.144	0.0327	0.146
λ_2	0.112	0.0483	0.102
λ_3	-1.58	-1.89	-2.35
λ_4	-1.19	-1.11	-0.74
λ_5	1.04	0.678	-0.458
λ_6	0.536	0.819	0.529
λ_7	-0.307	0.535	1.08
λ_8	0.264	0.227	0.229
λ_9	0.336	0.242	0.284

Table S1: Estimated coefficients for each of the covariates used in the gravity model (20), for each commodity. The high-dimensional coefficients κ_i and ω_j are not shown.

[*]Dairy products comprise: butter, skim milk of cows, cheese, other dairy products. [†]Sugar products comprise: sugar, refined sugar, syrups, fructose, sugar confectionery.

We consider the following gravity model for our comparison study [11]:

$$\log T_{ij} = \kappa_i + \omega_j + \lambda_1 \log O_i + \lambda_2 \log E_j + \lambda_3 \log d_{ij} + \lambda_4 \text{CNTG}_{ij} + \lambda_5 \text{CNLY}_{ij} + \lambda_6 \text{LANG}_{ij}$$
$$+ \lambda_7 \text{RTA}_{ij} + \lambda_8 \log \chi_j + \lambda_9 \log \text{TRFF}_{ij}. \tag{20}$$

The covariates 5–9 are taken from the CEPII database [36]:

1. κ_i are the time-dependent exporter-fixed effects,

2. ω_j are the time-dependent importer-fixed effects,

3. O_i is the total production output of the exporter, in tonnes, as given by the FAO.

4. E_j is the total consumption of the importer, in tonnes,

5. d_{ij} is the geodesic distance in km between the population centres of each country (harmonic average) (`distw_harmonic`),

6. CNTG indicates whether the two share a land border (`contig`),

7. CNLY is a binary variable indicating whether there ever existed colonial ties before 1948 between the two trading partners (`col_dep_ever`),

8. LANG indicates whether the two share an official or primary language (`comlang_off`),

9. RTA is a binary variable indicating whether there exists a bilateral regional trade agreement (`rta_coverage`, where the variable is 0 for `rta_coverage == 0` and 1 else),

10. $\chi_j = \sum_i d_{ij} O_i / \sum_k O_k$ is the remoteness index of the importer,

11. TRFF is the tariff applied by the importer in the absence of a trade agreement. We use the most favoured nation tariff (maximum duty) as given by the WTO [38]: `MFN - Maximum duty by product groups`.

The remoteness index accounts for the multilateral resistances [11]. This gives a $L \times (m + n) + 9$-dimensional regression problem for each commodity, where $L = 22$ are the number of years in the dataset (the fixed-effects are time-dependent). We estimate the parameters $\{\lambda_k\}$ using Poisson Pseudo Maximum Likelihood optimisation. Table S1 gives the estimated parameters for each commodity. Figure S1 plots the estimated values $\hat{T}_{ij}$ against the reporter-averaged FAOStat values for both the OT and the gravity models. Also shown are a linear fit with slopes and Pearson coefficients indicated.

A Barley
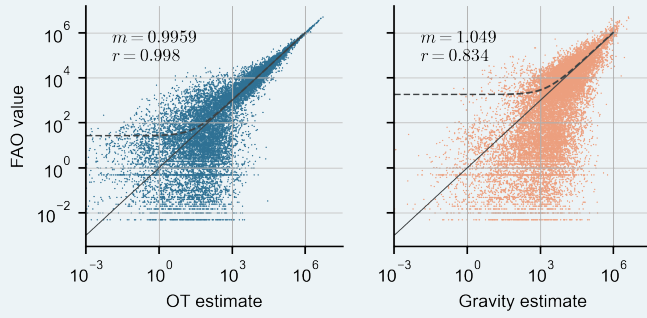
B Beef
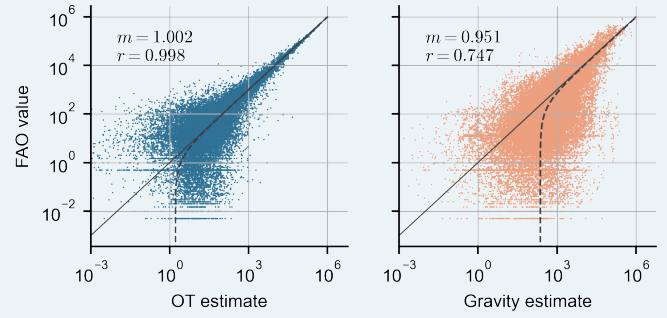
C Wine
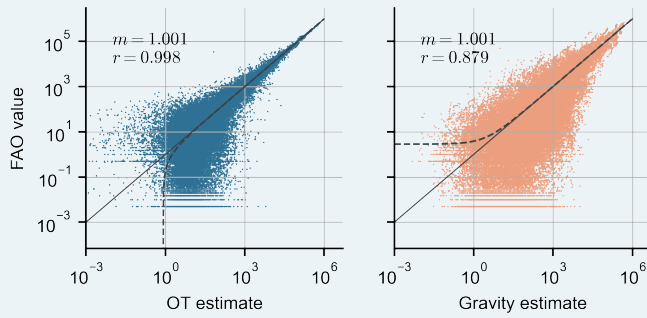
D Wheat
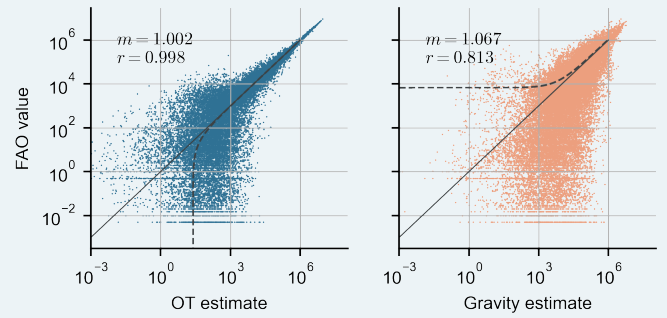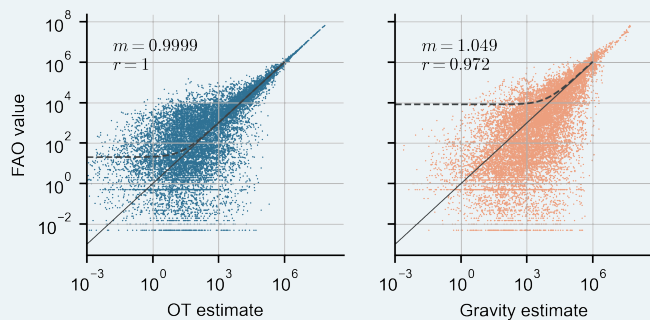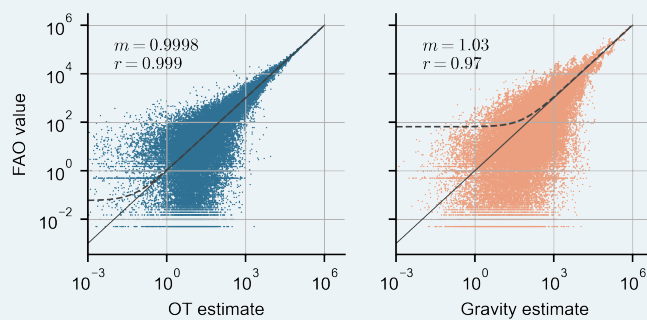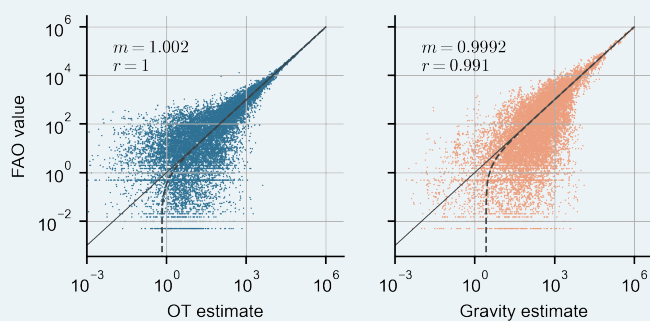
E Dairy products
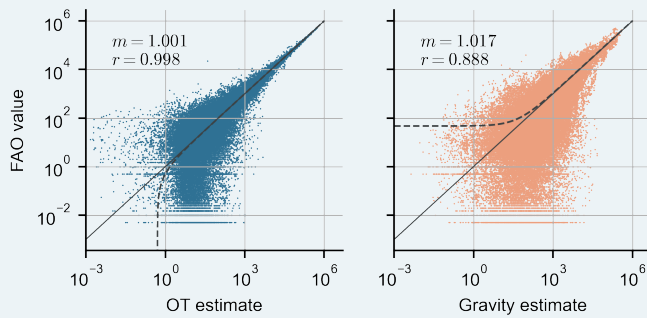
F Sugar products
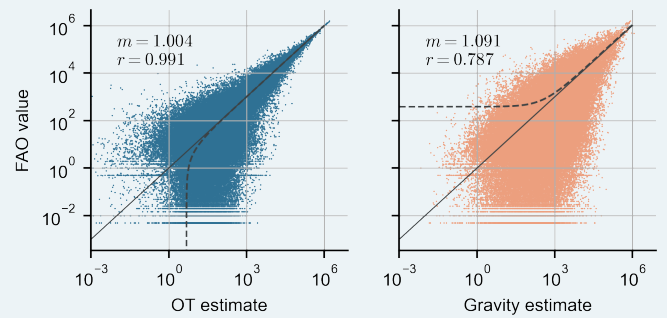
G Corn
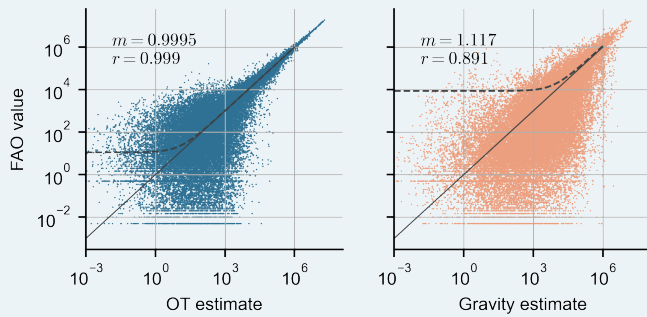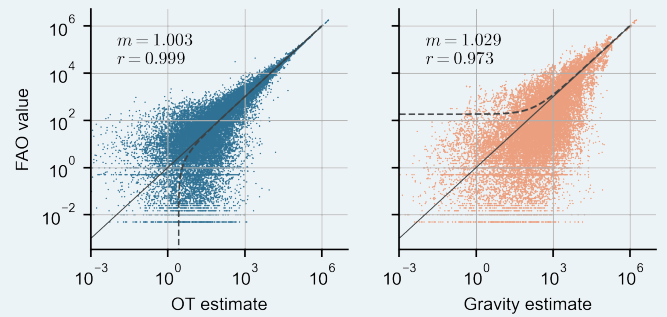
H Tomatoes

Figure S1: Comparison of the OT estimates (left, darkblue) and the Gravity estimates (orange) for each commodity. The y-axis shows the true FAO value, while the x-axis shows the estimated value. The solid line is the diagonal $y = x$. Also shown are a linear fit (dashed line) as well the fitted slope m and Pearson correlation r of the fit.